第 32 卷第 3 期
2016 年 3 月

无 机 化 学 学 报
CHINESE JOURNAL OF INORGANIC CHEMISTRY

Vol.32 No.3
491-498

$YAlO_3$ 的体色与缺陷平衡的关系

刘 勇[1] 刘天慧[1] 毕淑娴[2] 安 炜[3] 李国宝[4] 田光善[3] 焦 桓*,[1] 荆西平*,[4]

([1]陕西省大分子科学重点实验室,陕西师范大学化学与化工学院,西安 710062)

([2]宁夏大学化学化工学院,银川 750021)

([3]北京大学物理学院,北京 100871)

([4]稀土材料化学与应用国家重点实验室,北京大学化学与分子工程学院,北京 100871)

摘要: 利用固相扩散法在 1 450 ℃下制备了 $YAlO_3$ 粉末样品和陶瓷片样品,并在不同温度和不同气氛(air, O_2 or N_2)下对样品进行退火处理调制了其缺陷浓度。基于漫反射光谱和交流阻抗谱分析了 $YAlO_3$ 样品的体色与其缺陷浓度之间的关系。研究结果表明 $YAlO_3$ 具有 p 型导电机理,其浅棕色体色是由阳离子空位引起的。在高温和氮气氛下处理该材料其缺陷浓度减少,体色变浅。第一性原理计算结果认为 $YAlO_3$ 中的主要缺陷应该是铝空位 $V_{Al}^{\times}$。

关键词: $YAlO_3$; 体色; 阳离子空位; 漫反射光谱; 交流阻抗谱。

中图分类号: O614.51+1 **文献标识码**: A **文章编号**:1001-4861(2016)03-0491-08

DOI:10.11862/CJIC.2016.051

Correlation Between the Body Color of $YAlO_3$ and Its Defect Equilibrium

LIU Yong[1] LIU Tian-Hui[1] BI Shu-Xian[2] An Wei[3] LI Guo-Bao[4]

TIAN Guang-Shan[3] JIAO Huan*,[1] JING Xi-Ping*,[4]

([1]*Key Laboratory of Macromolecular Science of Shaanxi Province, College of Chemistry and Chemical Engineering, Shaanxi Normal University, Xi'an* 710062, *China*)

([2]*College of Chemistry and Chemical Engineering, Ningxia University, Yinchuan* 750021, *China*)

([3]School of Physics, Peking University, Beijing, 100871, *China*)

([4]*State Key Laboratory of Rare Earth Materials Chemistry and Applications, College of Chemistry and Molecular Engineering, Peking University, Beijing* 100871, *China*)

Abstract: Powder and pellet samples of $YAlO_3$ with various defect concentrations were prepared using conventional solid state reactions at 1 450 ℃, followed by annealing in air, O_2 or N_2 atmospheres at various temperatures. The correlation between the body-color of the samples and the defect equilibria was investigated by diffuse-reflection spectra and AC impedance data. The results indicate that $YAlO_3$ has p-type conduction and its light-brown body-color is caused by the cation vacancies. Annealing $YAlO_3$ at high temperature in N_2 atmosphere may reduce the defect concentration and the body-color. By the first-principle calculations, it is proposed that the Al vacancies $V_{Al}^{\times}$ may be the dominant defects in $YAlO_3$.

Keywords: $YAlO_3$; body-color; cation vacancy; diffuse~reflection spectrum; AC impedance

收稿日期:2015-07-24。收修改稿日期:2015-12-15。

国家自然科学基金(No.21371015)资助项目。

*通信联系人。E-mail:jiaohuan@snnu.edu.cn, xpjing@pku.edu.cn;会员登记号:S06N3161M1407。

0 Introduction

In the early studies on the defects, more attentions have been paid on the defects in alkali halides, such as sodium vacancy $V_{Na}^{\times}$ and chlorine vacancy $V_{Cl}^{\times}$[1]. Since these defects caused the colorless crystals colored, they were named as color centers (or *F*-centers). In fact, the defects are very important for material properties. As we know, the blue-greenish luminescence of ZnO originates from the zinc vacancy V_{Zn}'' and oxygen vacancy $V_O^{\cdot\cdot}$[2] and the conductivity and dielectric loss of some titanate microwave ceramics are affected by the oxygen vacancy $V_O^{\cdot\cdot}$ and trivalent titanium defect Ti_{Ti}'[3]. In recent years, a novel material——solid electride attracted many research interests[4]. A typical solid electride material is $[Ca_{12}Al_{14}O_{32}]^{2+}$:$[2e^-]$, which was prepared by heating its host material $Ca_{12}Al_{14}O_{33}$ in reductive atmospheres, such as CO/CO_2 and in which the $[2e^-]$ plays a role as an electron anion. Actually the $[2e^-]$ anion is another expression of the electron captured in the oxygen vacancy $V_O^{\times}$ (F-center), thus this electride material can be considered as the compound with high concentration of $V_O^{\times}$. Since $V_O^{\times}$ can contribute high concentration of loosely-bonded electrons, after reduction, this material changes from an insulator to a conductor, consequently it can be potentially used as a transparent electrode, low-temperature electron emitter, high-density optical storage[4-5]. These materials were also used as catalysts for the NH_3 syntheses and CO oxidation[6-7].

When previously studied the ternary phase diagram SrO-Y_2O_3-Al_2O_3 in our group[8], we found that $YAlO_3$ powder prepared by high temperature reaction always showed light-brown body-color. As we know, $YAlO_3$ is composed of Y^{3+}, Al^{3+} and O^{2-}, all of which have 8-electron full-shell configurations. Accordingly, this material should have a wide bandgap ($E_g \approx$ 7.1 eV[9]) and should not have absorption in visible range, so that it should be a colorless crystal or white powder. Therefore, it can be deduced the body-color of this material must arise from some defects. In this study, we attempt to know what defects cause the body-color in this material and how the body-color can be adjusted. Furthermore whether it is possibly to modify $YAlO_3$ as a material with high defect concentration, so that we can obtain another electride. On the other hand, $YAlO_3$ is a host material of a laser crystal. Some researches have been reported on growing single crystals of $YAlO_3$[10-13] It was found that the grown crystals also had light-brown body-color, which caused the crystal quality detriment. When the crystals were annealed in reductive atmospheres, their body-color was reduced. However, in the previously reported work, the mechanism of the body-color production was not properly discussed. If we could understand the generating mechanism of the body-color and find ways to reduce it, we would improve the quality of the crystal.

The $YAlO_3$ powder samples were prepared by solid state reactions at high temperature. X-ray diffraction indicated that besides a few percent of impurity phase $Y_4Al_2O_9$, the main phase in the samples was the expected $YAlO_3$, which showed light-brown body-color. The absorption spectra and conduction properties of the samples were characterized, and the formation energies of possible defects were calculated by the first-principle calculations. By analyzing the above data, it is indicated that the main defects in $YAlO_3$ are probably cation vacancies $V_{Al}^{\times}$, which cause its light-brown body-color and the p-type conduction.

1 Experimental and calculations

1.1 Sample preparation

Y_2O_3 (99.99 %) and γ-Al_2O_3 (luminescent pure) were used as raw materials. The raw materials in 1∶1 molar ratio were weighed and thoroughly ground in an agate mortar with pestle. In order to get homogeneous powder mixtures, a few drops of ethanol were added during the grindings. After grindings, the powder mixture samples were put in alumina crucibles, and calcined at 1 450 ℃ for 12 h in a muffle furnace. Intermediate grindings were applied during the calcination for improving the phase purity of the samples. After calcination, the samples were ground

into powders.

For conductivity measurements, sintered pellet samples were prepared. The powder samples were mixed with a few drops of 5%(*w*/*w*) polyvinyl alcohol solution as a binder, and then they were pressed into pellets with 10 MPa pressure in a stainless steel die. Finally, the as-pressed pellets were sintered at 1 450 ℃ for 12 h. The obtained sintered pellets had the dimension ~1.3 cm in diameter and ~0.2 cm in thickness with relative density ~88%. To investigate the influences of atmospheres to the body-color and the profile of the reflection spectrum, the powder samples were annealed in a tube furnace with O_2, air and N_2 atmospheres, respectively, at 700 ℃ or 1 450 ℃ for 4 h.

1.2 Characterizations

The phase purity of samples were determined by X-ray diffraction (XRD) using a Rigaku Dmax2000 X-ray powder diffractometer (Japan) with Cu $K\alpha$ radiation (λ=0.154 18 nm) at 40 kV and 100 mA. The XRD patterns were collected in the 2θ range 10°~60° with the scanning rate $8°\cdot min^{-1}$.

The diffusive reflection spectra were measured by using an ultraviolet-visible-near infrared(UV-Vis-NIR) spectrophotometer (Shimadzu UV-3100, Japan) in the range 240~1 000 nm and the $BaSO_4$ powder was used as reference.

The electrical properties of the samples were characterized by AC impedance spectroscopy using a Wayne Kerr-6500B impedance analyzer (Wayne kerr electronics Ltd, UK) in the frequency range 1 Hz to 10^7 Hz and the temperature range 200~800 ℃ with the temperature interval 20 ℃ / waiting time 20 min for each temperature point. Prior to the measurements, the Pt electrodes on the two opposite surfaces of the pellet samples were prepared by coating platinum paste with two Pt wires followed by heating at 800 ℃ for 10 min to burn off the organic components in the paste. The measured AC impedance data were analyzed using the Zview software[14].

1.3 First principle calculations

To acquire the defect formation energy, the energies (E_L) of the ideal structure of $YAlO_3$ and the structures with various defects were calculated using CASTEP (Cambridge Serial Total Energy Package, Accelrys Inc.) in Materials Studio 5.0[15]. The defect formation energy (E_V) is the energy difference (E_L) between the defective and the ideal structures. In these calculations, the density functional theory(DFT) with local-density approximation (LDA) was employed and the wave functions of valence electrons were expanded in an ultrasoft pseudopotential plane-wave basis sets with the specific cut-off energy E_{cut}. For the calculations, a 2×2×2 supercell (160 atoms) was chosen according to the ICSD file 99419. The initial supercell are $a^*=2a$=1.036 05 nm, $b^*=2b$=1.065 90 nm and $c^*=2c$=1.474 12 nm. Based on this supercell structure, the two defective structure modes were built by removing out one Y atom near the center in the supercell for $V_Y^{\times}$ and one Al atom for $V_{Al}^{\times}$, respectively. Before the energy calculations, the geometry optimization for each mode was performed with Broyden-Fletcher-Goldfarb-Shannon (BFGS) alogrithm[16]. Both E_{cut} and k-point mesh were tested and set as 260 eV and 3×3×2 Monkhorst-Pack grid, respectively, which are enough for energy convergence. The modes were converged when the force on each atom was less than $1\ eV\cdot nm^{-1}$ with a maximum displacement of 0.000 5 nm and a convergence in the total energy of about $5\times10^{-5}\ eV\cdot atom^{-1}$.

2 Results and discussion

2.1 Phase analysis

The prepared $YAlO_3$ powder samples had light-brown body-color. The XRD pattern of $YAlO_3$ is shown in Fig.1. The pattern is in accordance with JCPDS file 33-41, except for two weak peaks appearing at 2θ=29.18° and 31.26°, which are from the impurity phase $Y_4Al_2O_9$ (JCPDS file 14-0475). $YAlO_3$ has orthorhombic unit cell and the cell parameter calculated from the pattern in Figure 1 are as follows: a=0.518 8(1) nm, b=0.525 5(1) nm and c=0.738 5(1) nm. The material had a twisted perovskite structure with the space group *Pbnm* (No.62), which contains one Y site and one Al site (ICSD file 99419,

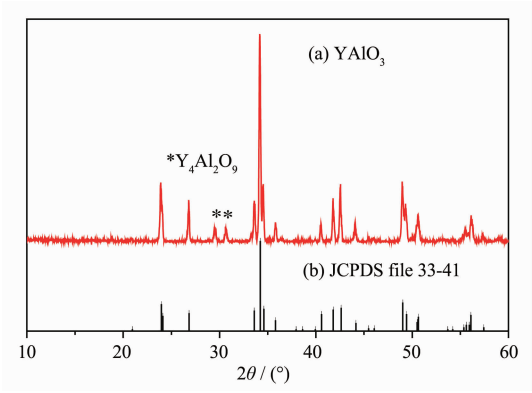

Fig.1 XRD patterns of as-prepared $YAlO_3$ (a) and JCPDS file 33-41 (b)

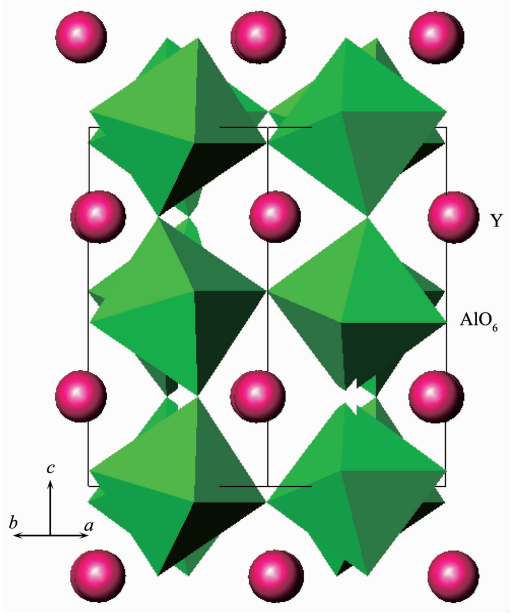

Fig.2 $YAlO_3$ perovskite structure

shown in Fig.2). In fact it was quite hard to obtain pure-phase $YAlO_3$ samples. Various preparation conditions were tested, such as modifying raw material ratio Y_2O_3:Al_2O_3, as well as enhancing the heating temperature and prolonging the heating time, the two weak XRD peaks of $Y_4Al_2O_9$ did not disappear. For comparison, a pure phase sample of $Y_4Al_2O_9$ was prepared by heating Y_2O_3 and Al_2O_3 mixture with the Y_2O_3:Al_2O_3 ratio 2:1 at 1 100 ℃ for 12 h. The XRD pattern of the prepared sample is in accordance with the JCPDS file 14-0475 and the body-color of the sample is white, thus we believe that the light-brown color of the prepared $YAlO_3$ sample is caused by $YAlO_3$ itself rather than $Y_4Al_2O_9$ and small amount of impurity phase $Y_4Al_2O_9$ may not seriously affect our results.

2.2 Diffusive reflection spectra

Fig.3 illustrates the diffusive reflection spectra of the $YAlO_3$ samples annealed in various atmospheres at 700 ℃ or 1 450 ℃. All the samples have absorption in the visible range 400~800 nm. The absorption in the blue range (*e.g.*~450 nm) is stronger than that in the red range(*e.g.*~650 nm), as the result, the samples shows light-brown body-color. The samples annealed in air and O_2 have much stronger absorptions(showing deeper body-color) than the samples annealed in N_2 (showing lighter body-color), these imply that the body color of $YAlO_3$ is caused by some defects, which can be adjusted by atmospheres. According to the correlation between the body-color and the atmospheres, it can be deduced that the defects should be anion excess defects, *e.g.* interstitial oxygen O_i or cation vacancies $V_M^{\times}$ ($V_Y^{\times}$ or $V_{Al}^{\times}$). The defect equilibria can be represented as the following reactions:

$$O_2 \rightleftharpoons 2O_i^{\times} \quad (1)$$

$$O_i^{\times} \rightleftharpoons O_i'' + 2h^{\cdot} \quad (2)$$

$$3O_2 \rightleftharpoons 6O_O^{\times} + 4V_M^{\times} \quad (3)$$

$$V_M^{\times} \rightleftharpoons V_M' + h^{\cdot} \ (M=Y \text{ or } Al) \quad (4)$$

When the electron transitions occur from valence band to the defects $O_i^{\times}$ and $V_M^{\times}$, they may be changed to O_i'' and V_M' and the electron holes $h^{\cdot}$ are produced in the valence band. V_M' may be further ionized to V_M'' and V_M''', and more $h^{\cdot}$ are produced. In these processes,

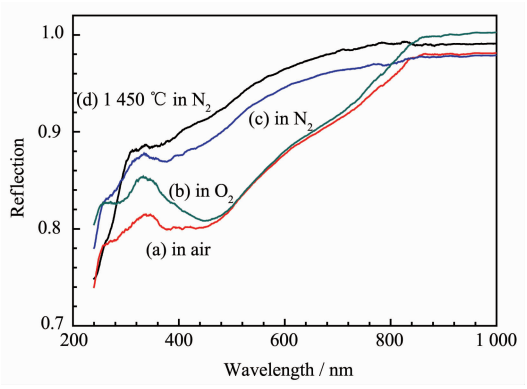

Fig.3 Diffusive reflection spectra of the $YAlO_3$ samples annealed in air(a), O_2(b) and N_2(c) at 700 ℃ and annealed in N_2 at 1 450 ℃(d)

Table 1　Optimized energies(E_L) of the unit cells and the defect formation energies(E_V)

	Ideal cell	$V_Y^{\times}$	$V_{Al}^{\times}$
E_L / eV	−9 717	−8 652	−9 646
E_V / eV		1 065	71

visible lights are absorbed by the material and the body-color appears. It is known that the $YAlO_3$ perovskite structure is stacked by the closely packed YO_3 layers in the cubic close packing sequence and the Al atoms are located at the octahedral interstitial sites constructed solely by the O atoms. In this kind of the structure, probably there is no space to accommodate O_i, so that we believe the main defects in $YAlO_3$ should be cation vacancies.

Further we have a discussion about which cation vacancy, $V_Y^{\times}$ or $V_{Al}^{\times}$ is the dominant defect. Fig.4 schematically represents the formation of a cation vacancy. In the atmosphere with high O_2 partial pressure, O_2 can be decomposed into O atoms and absorbed on the surface of the material, *e.g.* bonded to the Y atoms (two a atoms). At the same time, a cation vacancy V forms on the surface. Due to the thermal diffusion, both the Y atom and Al atom can jump from their own sites to the surface vacancy V and the cation vacancy may diffuse into the lattice. Here we use the ionic potential Z/r to evaluate the attracting strength of a cation to its surrounding oxygen atoms(Z is the valence and r is the radius of the cation). The larger the Z/r ratio, the stronger the attracting strength is. As we know, $r_{Y^{3+}}$=0.090 nm(CN=6), $r_{Al^{3+}}$=0.053 5 nm (CN=6)[17], as the results, the Z/r ratio for Y^{3+}(3.33) is less than that for Al^{3+}(5.61). This implies that Y^{3+} is easier to jump into the V site than Al^{3+}, thus it seems that $V_Y^{\times}$ is the dominant defect. However, the defect formation energy E_V of $V_Y^{\times}$ and $V_{Al}^{\times}$, calculated by the first-principle calculations, gives different result. E_L represents the optimized energies for different structural modes, including ideal supercell and the supercell with various cation defects. The defect formation energy E_V is the difference of E_L between the defective cell and the ideal cell. For the calculation, 2×2×2 supercell was used and the results are shown in Table 1. The data indicate that $V_{Al}^{\times}$ has much lower E_V than $V_Y^{\times}$, thus $V_{Al}^{\times}$ should be the dominant defect. As we know, Y^{3+} has much larger size than Al^{3+}, and the $V_Y^{\times}$ formation may cause larger lattice distortion and enhance the lattice energy, thus the first-principle calculation indicates that $V_{Al}^{\times}$ is the main defect in $YAlO_3$.

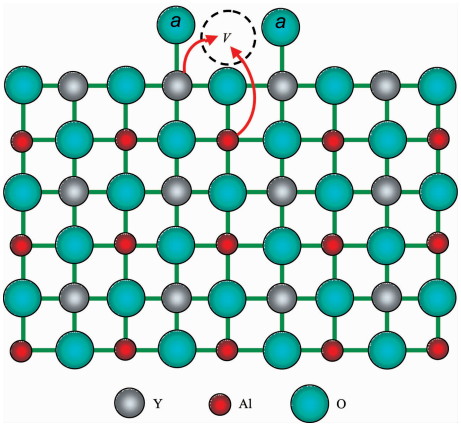

Fig.4　Schematic diagram for the defect formation

In the higher O_2 partial pressure (*e.g.* in O_2 atmosphere), Equilibria(**3**) and(**4**) shift to right, so that the concentration of $V_{Al}^{\times}$ increases and the body-color become deeper; while in N_2 atmosphere, the O_2 partial pressure is low, Equilibria (**3**) and (**4**) shift to left, consequently the concentration of $V_{Al}^{\times}$ decreases and the body-color become lighter. Equilibria (**3**) and (**4**) also show during the formation of $V_{Al}^{\times}$, gaseous O_2 is changed to solidus O^{2-}, which can be considered as an oxidezing reaction, thus probably it is an exothermal process (the enthalpy decreases, $\Delta H<0$) with the reduction of entropy ($\Delta S<0$). According to the Gibbs free energy equation $\Delta G=\Delta H-T\Delta S$, in order to reduce the concentration of $V_{Al}^{\times}$ in $YAlO_3$, *i.e.* to push Equilibrium(**3**) and(**4**) shift to left, besides annealing in N_2 atmo-sphere, enhancing the annealing temperature is also helpful. Therefore the sample annealed in N_2 at 1 450 ℃ has weaker absorption (Fig.3(d)) than other samples.

In order to obtain energy levels of the defects in

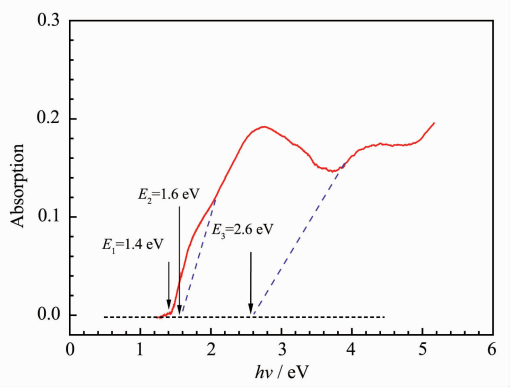

Fig.5 Reflection spectrum in the Absorption-$h\nu$ form for the $YAlO_3$ sample annealed in O_2 atmosphere at 700 ℃

$YAlO_3$, we further analyzed the reflection spectrum of the sample annealed in O_2 at 700 ℃, which has higher defect concentration. The spectrum is represented as the Absorption-$h\nu$ form (Fig.5), (h is Planck constant, and ν is the frequency of light). In the range 1.0 eV to 5.0 eV, three absorption peaks are observed, which correspond to three levels of the defects. The values of the energy levels were taken from the lower absorption edges of the corresponding absorption bands: 1.4, 1.6 and 2.6 eV. Yet at this stage we can not give exact assignments to these three levels, maybe they are related to the electron transitions from valence band to different ionized states of the Al vacancies: $V_{Al}^{\times}$, $V_{Al}^{'}$ and $V_{Al}^{''}$. The spectrum also shows the absorption above 5 eV, but we could not give further interpretation about this absorption because it is near the limit of the measurement. The Ref. [9] indicates the bandgap of $YAlO_3$ is about 7.1 eV, thus this absorption is not related to the band transition. Based on the above discussions, the band structure with the defect levels is illustrated in Fig.6.

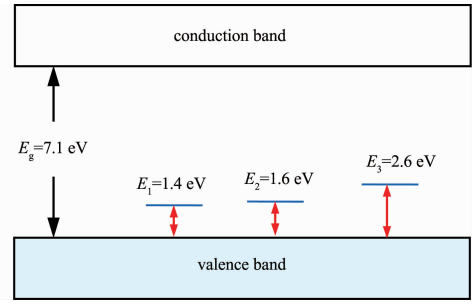

Fig.6 Band structure with defect levels of $YAlO_3$

Fig.6 shows that the bandgap of $YAlO_3$ is large, E_g =7.1 eV [9], thus the band transition may cause absorption in the vacuum ultraviolet (VUV) range, rather than in the visible range, which cannot lead to body-color appearance.

The cation vacancies produce three levels in the bandgap (although we can not give exact assignments for these levels at this stage). The electron transitions from the valence band to these levels (*i.e.* the electrons are captured at these levels from the valence band and the holes are produced in the valence band) cause absorptions in the visible to near infrared(near-IR) range, which may result in the body-color. The body-color of $YAlO_3$ has been previously reported by some authors, but they did not give clear explanation about this phenomenon[10-13]. We believe our above interpretation about the body-color of $YAlO_3$ is reasonable.

2.3 AC impedance analysis

It is mentioned above that the electron transitions from the valence band to the defect levels may cause the body-color of $YAlO_3$. On the other hand, these transitions also produce the holes in the valence band, resulting in p-type conductions, thus it is an effective way to analyze the defects by characterizing the conductance properties of the materials. In this work, the electrical conductivity of $YAlO_3$ was measured at various temperatures and in various atmospheres by AC impedance spectroscopy.

Fig.7 shows the typical Z''/Z' plot of $YAlO_3$ (at

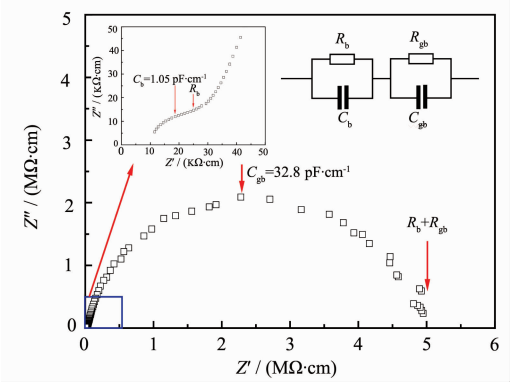

Inset is the enlarged view for the high frequency data

Fig.7 Typical AC impedance spectrum (Z''-Z' plot) of $YAlO_3$ at 560 ℃

560 ℃) and the simplified equivalent circuit. The large semicircle has the capacitivity 3.28×10^{-11} F·cm^{-1}, which is assigned as the grain boundary response, and the grain boundary resistivity (R_{gb}) can be extracted from the intercept of the grain boundary semicircle on the Z' axis. The grain boundary resistivity is much larger than the grain resistivity, thus the grain response is merged in the grain boundary response, and it can only be observed by enlarging the high frequency plot. The grain semicircle is not well resolved and the approximate value of the grain resistivity can be taken, as is shown, by the arrow in the inset.[18] The values of the grain resistivity at other temperatures were attracted by using the similar method.

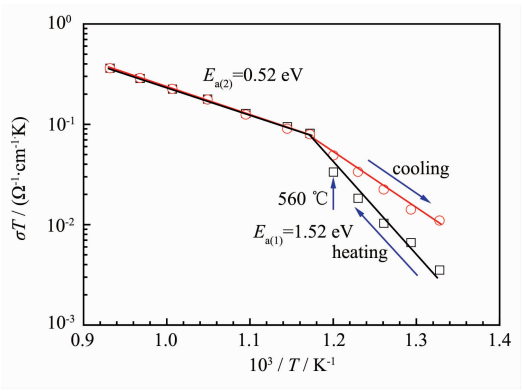

Prior to the measurements, the sample was quenched from 1 100 ℃

Fig.8　Arrhenius plots of the conductivity for $YAlO_3$ in the heating-cooling cycle

Fig.8 illustrates the Arrhenius plots of the conductivity for $YAlO_3$ in the heating-cooling cycle. At high temperatures (above 580 ℃), the defect reactions (**3**) and (**4**) are easier to approach to equilibrium. Whether in the heating or in the cooling process, at a certain temperature, the material has the same defect concentration, thus conductivities for both heating and cooling processes are almost identical. While at low temperatures (below 560 ℃), in the heating process since the $YAlO_3$ sample was previously quenched from 1 100 ℃, the defects formed during high temperature heating(*i.e.* 1 100 ℃) was "frozen" in the lattice at low temperatures (*i.e.* Equilibrium(**3**) was "frozen"). As the discussion in the 3.2 section, the defect reaction (**3**) is the entropy reducing process, thus the defect concentration of the sample quenched from high temperature is lower than that of the sample annealed in slow cooling process. Therefore, the conductivities in the heating process is lower than that in cooling process. Theoretically although the conductivities for the heating and cooling processes are different, their slopes in the Arrhenius plots should be identical. However, Fig.8 shows that the slopes of the plots at low temperatures are slightly different, possibly because at low temperatures, Equilibrium(**3**) is not completely "frozen".

By the Arrhenius plots, the activation energies for both low ($E_{a(1)}$) and high ($E_{a(2)}$) temperature ranges were calculated shown in Fig.8 (the data are the average values for the heating and cooling processes). $E_{a(1)}$ corresponds to the hole formation (Equilibrium(**4**), electron transition from the valence band to $V_{Al}^{\times}$). $E_{a(2)}$ corresponds to the two processes: the $V_{Al}^{\times}$ formation (correlated to Equilibrium(**3**) with the enthalpy change of ΔH) and the hole formation (correlated to $E_{a(1)}$), thus we have $E_{a(2)}=\Delta H+E_{a(1)}$. $E_{a(1)}$($\approx$1.52 eV) is very close to E_1 ($\approx$1.4 eV), indicating that the AC impedance data agree with the optical data well. Based on the above discussions, the enthalpy change of Equilibrium (**3**) can be calculated: ΔH=0.52 eV[$E_{a(2)}$]−1.52 eV[$E_{a(1)}$]=−1.00 eV=−96 kJ·mol^{-1}.

For further understanding the defect equilibrium, the conductivity variation of $YAlO_3$ with atmospheres was investigated. The measurements were conducted

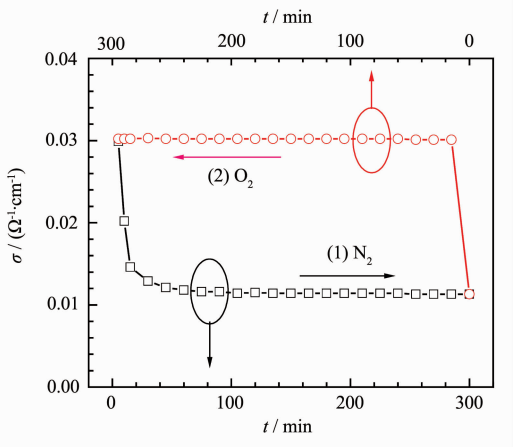

Fig.9　Variation of the bulk conductivity σ (at 720 ℃) with annealing time in atmospheres switched in the sequence: $N_2\rightarrow O_2$

at 720 ℃ and the data are represented in Fig.9. In N_2 atmosphere, the conductivity decreases rapidly in the first 75 min, and then it is almost constant in the following hours. Whereas when the atmosphere is switched to O_2, the conductivity increases rapidly. The data in Fig.9 further support that Equilibria (**3**) and(**4**) controls the defect concentration and the conductivity of $YAlO_3$.

Above results indicates that the defects in $YAlO_3$ are cation vacnacies, showing p-type conduction, thus this material is difficut to be modified to an electride as $[Ca_{12}Al_{14}O_{32}]^{2+}$:$[2e^-]$, which has n-type conduction. In fact, the conductivity of $YAlO_3$ is not high: at 600 ℃, its buck conductivity is only about 1.1×10^{-4} $\Omega^{-1}\cdot cm^{-1}$, much lower than that of $[Ca_{12}Al_{14}O_{32}]^{2+}$:$[2e^-]$($10^2$ $\Omega^{-1}\cdot cm^{-1}$ at room temperature).

3 Conclusions

The $YAlO_3$ samples with various defect concentrations were prepared by the solid state reactions at 1 450 ℃, followed by annealing in various atmospheres and at various temperatures. The defect levels and the defect equilibria were analyzed by the reflection spectra and AC impedance data. The results indicate that the light-brown body-color of $YAlO_3$ is caused by cation vacancies and the material has p-type conduction. The first-principle calculations show that the Al vacancies $V_{Al}^{\times}$ may be the domonent defect in $YAlO_3$, which may cause less lattice distortion. Annealing $YAlO_3$ in N_2 at high temperature may reduce the $V_{Al}^{\times}$ concentration and the body-color, which may supply a method to improve the quality of the $YAlO_3$ crystals.

References:

[1] Mott N F, Gurney R W. *Electronic Processes in Ionic Crystals*. 2*nd Ed*. Oxford: Clarendon Press, **1948**.

[2] Liu Z S, Jing X P, Wang L X, et al. *J. Electrochem. Soc*., **2006**,**153**(12):G1035-G1038

[3] Zhu H, Kuang X J, Jing X P, et al. *Jpn. J. Appl. Phys*., **2011**,**50**:065806

[4] Matsuishi S, Toda Y, Hosono H, et al. *Science*, **2003**,**301**: 626-629

[5] Kim S W, Shimoyama T, Hosono H, et al. *Science*, **2011**, 333:71-74

[6] Inoue Y, Kitano M, Hosono H, et al. *ACS Catal*., **2014**,**4**: 674-680

[7] Sharif M J, Kitano M, Hosono H, et al. *J. Phys. Chem. C*, **2015**,**119**:11725-11731

[8] Wang C H, Lin J H, Jing X P, et al. *J. Solid State Chem.*, **2012**,**192**:195-200

[9] Tomiki T, Kaminao M, Fukudome F, et al. *J. Phys. Soc. Jpn.*, **1991**,**60**(5):1799-1813

[10]LI Tao(李涛), ZHAO Guang-Jun(赵广军), PAN Shou-Kui (潘守夔), et al. *J. Synth. Cryst*.(人工晶体学报), **2002**,**31**(5): 456-459

[11]Weber M J, Bass M, Comperchio E, et al. *Appl. Phys. Lett*., **1969**,**15**:342-345

[12]Bernhardt H J. *Phys. Stattus Solidi A*, **1974**,**21**:95-98

[13]Chen J Y, Zhao G J, Cao D H, et al. *Current Appl. Phys*., **2010**,**10**:468-470

[14]*Zview for Windows*, *Impedance/Gain Phase Graphing and Analysis Software*, *Version* 1.4*b*, Scribner Associates Inc., Char-lottesville,Virginia, **1996**.

[15]Clark S J, Segall M D, Payne M C, et al. *Z. Kristallogr*., **2005**,**220**:567-570

[16]Pfrommer B G, Louie S G, Cohen M L. *J. Comput. Phys*., **1997**,**131**:233-240

[17]Shannon R D. *Acta Crystallogr*., **1976**,A32:751-767

[18]Irvin J T S, Sinclair D C, West A R. *Adv. Mater*., **1990**,**2**(3): 132-138